INTERNATIONAL JOURNAL FOR NUMERICAL METHODS IN FLUIDS, VOL. 18, 629–646 (1994)

NUMERICAL INVESTIGATIONS OF RADIAL JET REATTACHMENT FLOWS

H. LASCHEFSKI, D. BRAESS,* H. HANEKE AND N. K. MITRA†

Institut für Thermo- und Fluiddynamik (Department of Mathematics), Ruhr-Universität Bochum, Postfach 10 21 48, W-44721 Bochum, Germany*

SUMMARY

A finite volume computational scheme to solve the Navier–Stokes equations for the laminar flow fields of partially enclosed axial and radial jets impinging on a flat plate has been devised and tested. This scheme is based on the SIMPLEC technique. However, because of the backflow at the 'outflow' boundary, the SIMPLEC pressure correction technique has to be modified. The need for this modification, necessitated by the convergence failure, showed the 'hidden' pressure boundary condition of SIMPLE-type techniques. Test computations with the present scheme for flows in a channel with a built-in cylinder show that the location of the exit boundary affects very slightly the separated flow behind the cylinder. Computed Squire jet flows compare quite well with the available analytical solution. Finally, impinging radial jets have been computed for different Reynolds numbers. The results show the critical Reynolds number below which a steady solution is obtained and above which periodic and eventually chaotic flows result.

KEY WORDS Radial jet reattachment Pressure boundary condition

1. INTRODUCTION

Jets impining on a surface can result in large heat or mass transfer at the point of impingement. Hence they find important practical applications in the heating, cooling or drying of product surfaces in the paper, glass, metal and textile industries. The jets discharge from round or rectangular slots and often a bank of such jets is used in application. These jets can be axial or radial (see Figures 1 and 2).

An axial jet (Figure 1) impinging on a flat plate produces a very large transfer coefficient at the reattachment point. Away from the reattachment point the transfer coefficient decreases rapidly. A radial jet (Figure 2) discharges from the side of the feed tube and reattaches on the impinging plate because of the Coanda effect. Here, instead of a reattachment point, one obtains a reattachment line in the form of a closed curve. The transfer coefficient is moderately high on the reattachment line and decreases away from it. For a round feed tube the radius of the reattachment circle depends on the geometrical and flow parameters. The main advantage of a radial jet is that the moderately high heat or mass transfer can be distributed over a larger area than for an axial jet; the size and location of this area as well as the flux density can be easily controlled by changing the geometrical parameters (e.g. h, the distance between the jet and the impinging plate) or flow parameters (e.g. the Reynolds number at the jet discharge). For an axial jet these parameters can essentially change the flux density at the reattachment point.

A large number of experimental investigations of heat and mass transfer on a surface by a single or a bank of round or rectangular axial jets have been carried out by a group at the

CCC 0271–2091/94/070629–18

Received April 1993
Revised November 1993

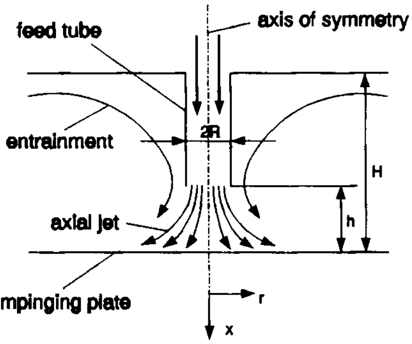

Figure 1. Schematic diagram of axial impinging jet

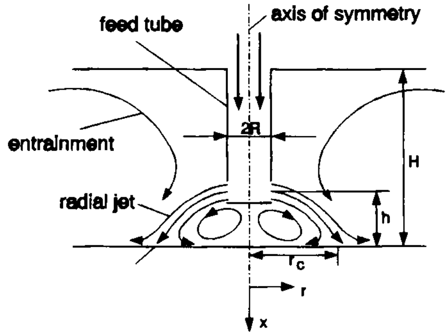

Figure 2. Schematic diagram of radial jet

University of Karlsruhe. The results with empirical formulae for the Nusselt and Sherwood numbers have been summarized by Martin.[1]

For laminar and turbulent radial jets impinging on a plate, Page *et al.*[2] made an analytical study of reattachment assuming that the velocity profile of the jet can be described by the boundary layer theory. Their results predict reasonably well the reattachment radius of the turbulent jet, but they cannot predict the near or far fields of the flow. Ostowari *et al.*[3] have presented experimental results of heat transfer on the impinging plate for turbulent radial jets.

The optimum application of impinging jets for maximum heat and mass transfer depends on the flow structure, which in turn depends on the geometrical parameters such as R, h, L (see Figures 1 and 2) and the angle of inclination of the jet exit with respect to the impinging plate. The flow structure of a reattaching jet is complex, especially that of a reattaching radial jet, since a separation bubble in the form of a vortex ring will appear around the axis below the feed tube. The shape and size of this vortex ring as well as the radius of the reattachment circle depend on the geometry, angle of inclination and Reynolds number. The effect of the Reynolds number is even more complicated, since at a sufficiently high Reynolds number the laminar jet may undergo a transition to turbulence before or after hitting the impinging surface. For an axial jet the peak value of heat transfer may appear downstream of the reattachment point.[1] The transition to turbulence after the reattachment on the impinging plate may be the reason. As a turbulent jet spreads radially after impinging, the cross-sectional area of the flow increases, thereby reducing the velocity. This may result in a relaminarization of the flow. An impinging radial jet may show self-sustained oscillation. Ostowari *et al.*[3] observed inherent non-steadiness of the reattachment location of turbulent radial jets.

The complete near- and far-field flow structure of impinging jets can be simulated only by solving the full, non-steady Navier–Stokes and energy equations. The results will show seperated zones and steady or unsteady reattachment. The main difficulty in computing the flow field of an impinging jet comes from the entrainment. The solid walls (e.g. the impinging plate) and the inflow boundary of the jet exit are clearly defined for the computational domain. The rest of the boundaries are free. However, they cannot be handled as outflow boundaries. Through some parts of the boundaries the fluid is sucked into the computational domain, while through other parts the fluid leaves the computational domain. This behaviour of the flow has been observed by Page *et al.*[2] and Ostowari *et al.*[3]

The purpose of the present work is the development of a computational scheme for Navier–Stokes and energy equations and numerical simulations of axial and radial jets with impinging plates. The computational scheme is based on the SIMPLEC procedure of van Doormal and Raithby.[4] It is shown that for the present geometry the pressure correction of the SIMPLE-type[5] procedure fails to converge. An investigation of this failure shows the pressure boundary conditions implicitly used in SIMPLE and the modifications of the pressure scheme required for the convergence.

In the present work only laminar jets are considered, since the computational scheme developed for a laminar jet can be easily used for turbulent jets when the turbulence is described by some model equations (e.g. the k–ε model). Furthermore, computational results are obtained for partially enclosed jets (see Figures 1 and 2), since such jets are often used in practice (e.g. electronic cooling and drying). The partial enclosure of the jet by putting a wall on the top solves the problem of specifying the boundary conditions on the top. However, flow reversal still takes place at the free boundary. For the validation of the computational scheme, the flow of a Squire jet[6] has also been computed and compared with the analytical solution.

2. BASIC EQUATIONS AND BOUNDARY CONDITIONS

2.1. *Basic equations*

The flow field of a radial jet is assumed to be axisymmetric and is described by the continuity and momentum (Navier–Stokes) equations in cylindrical polar co-ordinates (see Figures 1 and 2). The basic equations written in non-steady form for an incompressible fluid are: *continuity* equation,

$$\frac{\partial(ur)}{\partial x}+\frac{\partial(vr)}{\partial r}=0; \tag{1}$$

axial momentum equation,

$$\frac{\partial u}{\partial t}+u\frac{\partial u}{\partial x}+v\frac{\partial u}{\partial r}=-\frac{1}{\rho}\frac{\partial p}{\partial x}+\frac{\mu}{\rho}\left[\frac{1}{r}\frac{\partial}{\partial r}\left(r\frac{\partial u}{\partial r}\right)+\frac{\partial^2 u}{\partial x^2}\right]; \tag{2}$$

radial momentum equation,

$$\frac{\partial v}{\partial t}+u\frac{\partial v}{\partial x}+v\frac{\partial v}{\partial r}=-\frac{1}{\rho}\frac{\partial p}{\partial r}+\frac{\mu}{\rho}\left[\frac{\partial}{\partial r}\left(\frac{1}{r}\frac{\partial(rv)}{\partial r}\right)+\frac{\partial^2 v}{\partial x^2}\right]. \tag{3}$$

Here u and v are axial and radial velocity components respectively, p is the pressure, ρ is the density, μ is the viscosity and t, x, and r are time, axial and radial co-ordinates respectively. The basic equations are non-dimensionalized as $\bar{u} = u/u_{\mathrm{av}}$, $\bar{v} = v/u_{\mathrm{av}}$, $\bar{p} = (p - p_{\mathrm{ref}})/\rho u_{\mathrm{av}}^2$, $\bar{x} = x/R$, $\bar{r} = r/R$, $\bar{L} = L/R$, $\bar{h} = h/R$ and $\bar{H} = H/R$, where u_{av} is the average velocity at the exist and p_{ref} is the reference pressure. The dimensionless equations contain as parameters the Reynolds number $Re = u_{\mathrm{av}}R/\nu$. The non-dimensional equations will not be presented here.

2.2 *Boundary conditions*

Figure 3 shows the computational domain for the radial jet.

No-slip conditions on the solid walls give

$$u = 0, \tag{4a}$$

$$v = 0. \tag{4b}$$

At the jet discharge measured or physically feasible velocity profiles for u and v can be used. We have carried out computations with both parabolic and uniform (top-hat) profiles at the exit. There is not much qualitative difference in the flow structure but some quantitative difference in the wall shear. More accurate computations should include the feed tube. However, this has been avoided in order to reduce the computational cost. In the present computations we have assumed a parabolic profile at the feed tube exit. The main problem is the specification of the nominal outflow boundary condition at CD in Figure 3, since this boundary condition should allow for the ambient fluid to be sucked into the computational domain across the upper part of the boundary and to leave the computational domain across the lower part of CD.

The computational results should be reasonably independent of the value of L or the position of CD. This problem of the outflow boundary condition has been discussed by Rannacher,[7] who suggested a 'natural' condition which in non-dimensional form is given as

$$\partial_n \vec{\mathbf{v}} + p = 0, \tag{5}$$

where ∂_n stands for the gradient of the velocity vector $\vec{v}$ in the normal direction to the boundary. For non-dimensional $p = 0$ one obtains $\partial_n \vec{v} = 0$. In other words, if the exit pressure is constant, the velocity gradient in the normal direction at the exit is zero. The discussion in the next section on the 'hidden' boundary condition for the pressure will show that a modification of the computational scheme with constant pressure at the exit is required in order to obtain a solution.

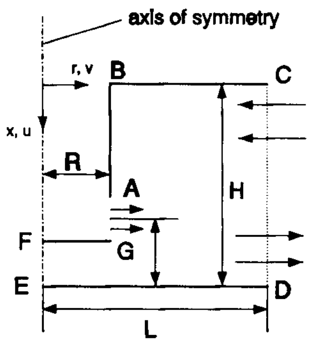

Figure 3. Computational domain for radial jet

Computational tests of flow fields in a channel with an obstacle (von Karman vortex street) show that the boundary condition (5) is independent of the length of the computational domain.[8] Such tests have also been performed in the present work.

3. METHOD OF SOLUTION

The basic equations are solved numerically by a modified SIMPLEC-based[4] finite volume technique on collocated grids (see Figure 4). For the discretization of the momentum equations central differences have been used for the viscous fluxes. The convective fluxes have been determined through the deferred correction approach first suggested by Khosla and Rubin.[9] According to this technique, the convective flux I_c is split into an implicit part expressed through a upwind difference scheme (UDS) and an explicit part containing the difference between the central difference scheme (CDS) and UDS approximations:

$$I_c^{n+1} = (\mathrm{UDS})^{n+1} + \Phi(\mathrm{CDS} - \mathrm{UDS})^n. \tag{6}$$

Here Φ is the flux-bending factor and n is the time level. When an iteratively converged solution for level $n+1$ is obtained, the discretization of equation (6) becomes tantamount to a second-order-accurate scheme. For a time-explicit non-iterative solution with $\Phi = 1$ we obtain second-order accuracy of central differences.

The flow field is obtained in two steps: in the first step the momentum equations are solved for a known pressure field; in the second step the solution of the continuity equation is obtained in an indirect way. A pressure–velocity correction in each discrete cell is performed in order to obtain a locally solenoidal velocity field. In order to avoid pressure oscillations of collocated grids, the momentum interpolation technique suggested by Maliska and Raithby[10] has been used in the pressure–velocity correction. It is this pressure–velocity correction technique that distinguishes between the original marker-and-cell (MAC) technique,[11] SOLA,[12] SIMPLE[4,5] and its derivatives.

For the present problem the SIMPLE scheme of pressure correction failed to converge because of the backflow across the nominal exit boundary CD (see Figure 3). In order to understand why SIMPLE fails, we look into the details of how SIMPLE works; in particular, we look into the implicit or 'hidden' pressure boundary condition[13] that SIMPLE uses.

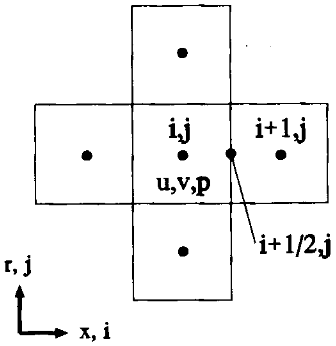

Figure 4. Collocated grid

Following the notation of Reference 5, the discretized x-momentum equation is written as

$$a_{i,j}u_{i,j} - \sum a_{\mathrm{nb}}u_{\mathrm{nb}} = -(p_{i+1/2,j} - p_{i-1/2,j})\Delta r + b_{i,j}. \tag{7}$$

Writing $u = u^* + u'$ in equation (7), where u^* is the value of u before and u' after correction due to the iteration, and neglecting $\sum a_{\mathrm{nb}}u'_{\mathrm{nb}}$ (SIMPLE assumption), one obtains

$$u'_{i,j} = \frac{(-p'_{i+1/2,j} + p'_{i-1/2,j})\Delta r}{a_{i,j}}. \tag{8}$$

Similarly the r-momentum equation gives

$$v'_{i,j} = \frac{(-p'_{i,j+1/2} + p'_{i,j-1/2})\Delta x}{a_{i,j}} \tag{9}$$

and the continuity equation gives

$$[(ru')_{i+1/2,j} - (ru')_{i-1/2,j})\Delta r - [(rv')_{i,j+1/2} - (rv')_{i,j-1/2}]\Delta x = -D_{i,j}, \tag{10}$$

where $D_{i,j}$ is the residual divergence in the cell. Equations (8)–(10) can be combined to obtain

$$\begin{aligned} p'_{i,j}&\left(-\frac{\Delta r^2}{a_{i+1/2,j}} - \frac{\Delta r^2}{a_{i-1/2,j}} - \frac{\Delta x^2}{a_{i,j+1/2}} - \frac{\Delta x^2}{a_{i,j-1/2}}\right)\\ -p'_{i+1,j}&\left(-\frac{\Delta r^2}{a_{i+1/2,j}}\right)\\ -p'_{i-1,j}&\left(-\frac{\Delta r^2}{a_{i-1/2,j}}\right)\\ -p'_{i,j+1}&\left(-\frac{\Delta x^2}{a_{i,j+1/2}}\right)\\ -p'_{i,j-1}&\left(-\frac{\Delta x^2}{a_{i,j-1/2}}\right) = D_{i,j}. \end{aligned} \tag{11}$$

This pentadiagonal equation is the pressure correction equation. Its main diagonal coefficients are the sum of the off-diagonal coefficients. This guarantees the diagonal dominance of equation (11).

The relation between the coefficients of equation (11) and the discretized momentum equation (7) should be noticed. When the coefficients of equation (7) are interpolated on the cell boundary, the reciprocals of these interpolated values are the coefficients of equation (11). A problem appears on the boundary. If $(i+\frac{1}{2}, j)$ is a point on the boundary (see Figure 4), the coefficient $a_{i+1/2j}$ is undetermined, since it cannot be interpolated from the node $(i+1, j)$ which lies outside the computational domain. Equation (11) can be easily solved if one assumes

$$p'_{i+1,j} = p'_{i,j}. \tag{12}$$

This reduces to the condition

$$\partial p'/\partial n = 0, \tag{13}$$

i.e. the normal gradient of the *pressure correction* is zero on the boundaries. Equation (12) also implies that the velocity on the boundary cannot be corrected (see equation (8)). This is perfectly acceptable on solid walls with the no-slip condition or for the Dirichlet condition in general, but not on a boundary where the flow velocity or direction is not known *a priori*. In the original SIMPLE algorithm[5] the velocity correction at the outflow boundary of the internal flow is performed by imposing global continuity condition there.[4] This is not possible when a backflow at the exit appears, since then the global mass flow is not *a priori* known. It should also be mentioned that the use of conservation of global mass flow makes equation (8) overdetermined.[4]

This problem of the pressure–velocity correction on the outflow boundary can be resolved if one uses instead of equation (13) a constant pressure on the boundary. This implies zero pressure correction on the boundary. If the boundary is denoted by $(i+\frac{1}{2}, j)$, the term $p'_{i+1,j}$ in equation (11) is set to zero, since the node $(i+1, j)$ lies outside the boundary. However, $p'_{i,j}$ lies inside the computational domain. The $(a_{i+1/2,j})^{-1}$ for this term is calculated from a linear extrapolation of the coefficients at (i, j) and $(i-1, j)$. Even with p_{CD} = constant, equations (8) and (9) can be used for the velocity correction on the 'outflow' boundary without imposing global continuity. Once the velocity field is obtained, the global continuity can be used to check the accuracy of the solution.

Chuang and Wei[14] computed semi-enclosed compressible turbulent impinging jets with the SIMPLEC algorithm. They have not pointed out any necessary modification of the algorithm. It should be noted that for compressible flows the pressure is not decoupled from the velocity field. Hence the pressure–velocity correction to satisfy the continuity equation has a different implication than for incompressible flow. The success of Chuang and Wei[14] in the computation of compressible flows does not imply that incompressible flows in the same geometries can be calculated by the method of reference 14. Furthermore, it should also be noted that SIMPLEC requires a modification of the pressure correction when substantial backflow at the exit appears. For a small amount of backflow the velocity correction at the exit cells can possibly be performed using the global continuity condition.[4] This will naturally reduce the accuracy of computations. The results of reference 14 do not indicate much backflow at the exit.

To summarize, we note that for the present problem a constant pressure at the exit (p_{CD} = constant) is the correct boundary condition for the pressure. This is consistent with equation (5).

The computations have been carried out on meshes of 102×202 and 102×402 for the test case of a square cylinder in channels of length $L = 10$ and 20. Test computations for one case show that the Strouhal number S computed with a grid of 102×202 differs from the grid-independent S by less than 4%.

The impinging free jets have been computed with grid of 194×322. Although the present code is able to compute time-implicit results iteratively, we have done here only time-explicit computations. The time step Δt has been chosen to satisfy the Courant–Friedrich–Lewy (CFL) condition for stability and the grid Fourier number restriction. One test case of the flow in a channel with a rectangular cylinder was calculated with the time step obtained from the stability condition and a reduced (50%) time step. The difference in Strouhal number was less than 3%.

4. RESULTS AND DISCUSSION

4.1. Test computations for flows in a channel with an obstacle

A large number of test cases have been computed with the present scheme. In order to determine whether the present scheme can handle unsteady, oscillatory flows, computations are first performed for two-dimensional flows in a channel with a square cylinder in the middle for $Re = 250$. This Reynolds number is based on the cylinder height. Figure 5 shows a schematic

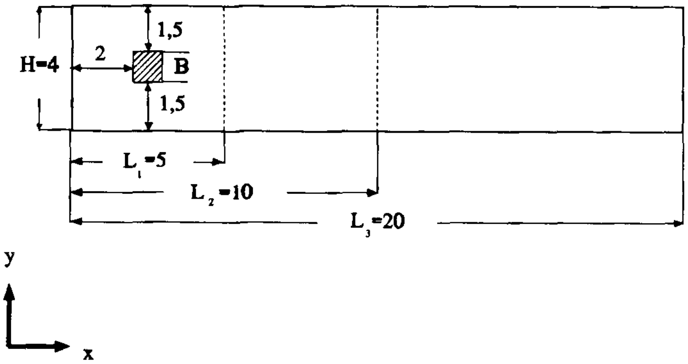

Figure 5. Schematic diagram of computational domain of 2D channel with square cylinder

diagram of the computational domain. All the lengths are non-dimensionalized with the cylinder height. At the channel entry a parabolic profile for u is used. The computations are performed in channels of non-dimensional lengths $L = 10$ and 20. The flow in the cylinder wake is oscillatory and the Strouhal number S based on the cylinder height and the average velocity is found to be 0·174 for both $L = 10$ and 20. Figures 6 and 7 show the contours of the lines of constant u and v in the wake of the cylinder up to a length $L = 10$. The double lines represent the results for $L = 10$ and 20. They show that the flow structures are absolutely identical qualitatively and almost identical quantitatively irrespective of whether the exit boundary conditions is applied at $L = 10$ or 20.

4.2. Computations of Squire jets

Further test computations are performed for Squire jets.[6] These are radial jets (see Figure 8) for which Squire[6] gave an approximately analytical similar solution. Figure 9 compares the halfwidths of the jet ($\Theta = 90°$) for $Re = 50$, 100 and 500. The Reynolds number here is based on the average velocity u_{av} at the tube discharge and the height of the opening, d. In the analytical solution of the Squire jet a point source at the feed tube axis has been assumed (see Figure 8), but in the numerical solution the flow at the tube discharge is assumed to have a parabolic profile. Hence precisely at the jet exit the halfwidths of the Squire solution and the numerical solution do not agree well. However, at $\bar{r} = r/d \geq 4$ the two solutions are indistinguishable from each other.

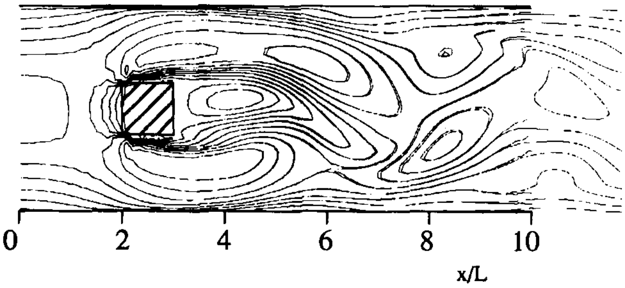

Figure 6. Superimposed contour lines of constant u-velocity for computations with exit boundary condition applied at $L = 10$ and 20

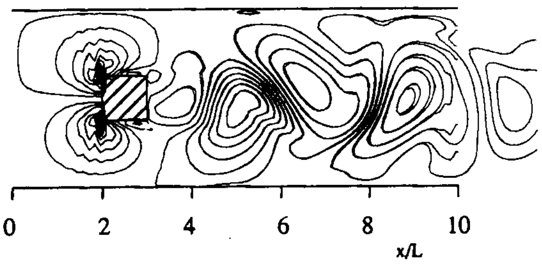

Figure 7. Superimposed contour lines of constant v-velocity for computations with exit boundary condition applied at $L = 10$ and 20

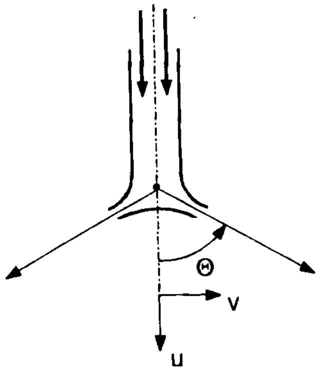

Figure 8. Schematic diagram of Squire jet[6]

4.3. Computations of impinging jets

A number of semi-enclosed laminar axial and radial jets impinging on a flat plate have been computed.

Figures 10(a) and 10(b) show a typical velocity vector plot and streaklines respectively of a semi-enclosed radial jet impinging on a flat plate. The Reynolds number Re based on the average velocity at the exit and the exit height R is 500. The non-dimensional distance between the feed tube and the plate is $h = 2$. At the exit of the computational domain, ambient fluid flows into the computational domain near the top and out of it at the bottom near the impinging plate. A separated dead-water zone appears directly below the feed tube. It is bounded by a tyre-shaped vortex ring. The streaklines (Figure 10(b)) show the vortex structure clearly. The influence of the Reynolds number for the particular geometry of Figure 10 has been thoroughly investigated. It was observed that when Re exceeded a certain critical value Re_c, a steady solution of the unsteady equations could not be obtained. The value of Re_c is also strongly dependent on the upwind fraction of the flux-blending difference for the convective term. The reattachment radius naturally depends strongly on the flow Reynolds number. Figure 11 shows the non-dimensional reattachment radius r_{re}/R versus the Reynolds number for different upwind fraction Φ. For approximately full central differencing ($\Phi = 0{\cdot}9$) the critical Reynolds number is 675. With $\Phi = 0{\cdot}1$ this critical Re is 950. It is interesting to note that Re_c depends linearly on Φ (see

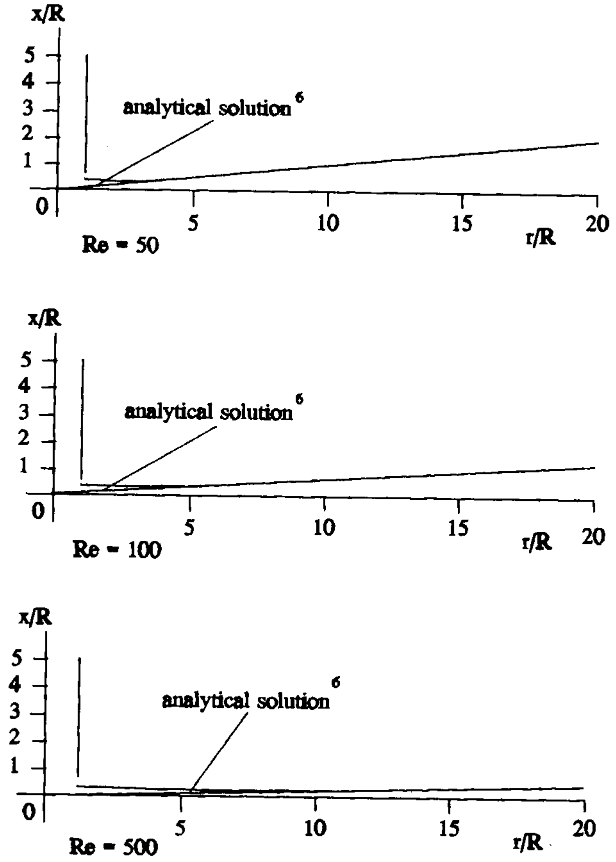

Figure 9. Comparison of analytical solution[6] and present computations of halfwidth distribution of Squire jet

Figure 12). For $\Phi = 1$ (fully central space differencing) one obtains from extrapolation of the curve in Figure 12 $Re_c = 634$. The lower curve shows the fraction of numerical viscosity as a function of the upwind fraction Φ. This has been obtained by assuming that the central differences possess zero numerical viscosity and the computed Re_c signifies the sum of physical and numerical viscosities. For 90% upwind ($\Phi = 0{\cdot}1$) the numerical viscosity ν_N/ν is 33% and for $\Phi = 0{\cdot}9$ ν_N/ν is less than 3%.

The computations break down (diverge) with $\Phi = 1$. Hence further computations have been performed for the non-steady cases with $\Phi = 0{\cdot}9$. It is observed that a periodic flow field is obtained up to an Re of 760. This periodicity can be quite clearly discerned by observing the wall shear on the plate. The reattachment radius moves periodically by nearly 5%.

For the periodic flow for $Re = 720$ the velocity components u and v at the location $x/R = 0{\cdot}025$, $r/R = 6{\cdot}5$ have been recorded over a period of time. Figure 13 shows the time series for the v-component. Figures 14 show the corresponding frequency analysis. A dominant frequency is apparent. The Strouhal number $S = fR/u_{av}$ is 0·05.

Figures 15(a) and 15(b) show streaklines and velocity vectors at different non-dimensional times $\tau = tu_{av}/R$ for $Re = 800$. The flow structure has changed completely. A non-steady non-periodic flow field is obtained. Figures 15(a1) and 15(b1) show that at $\tau = 0$ the jet comes

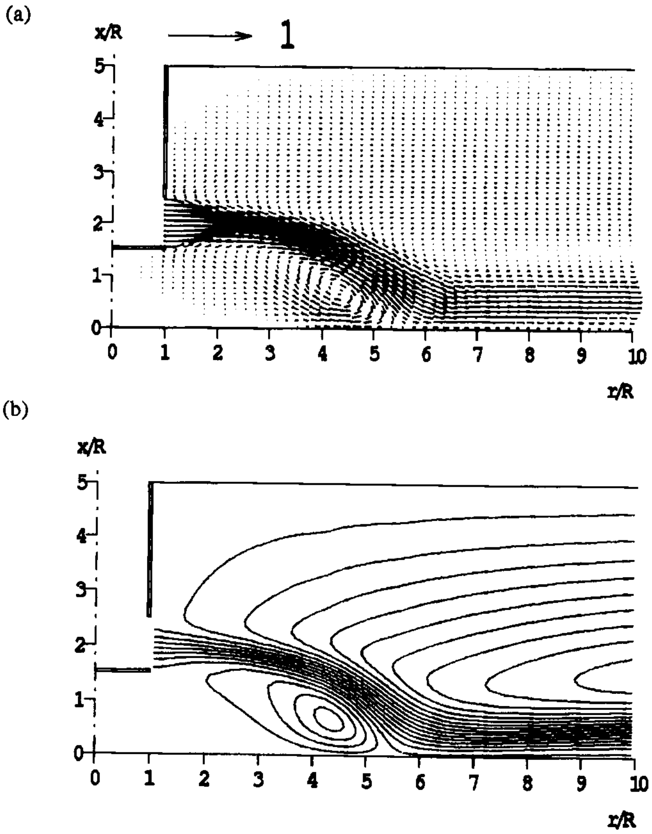

Figure 10. Typical (a) velocity vectors and (b) streaklines showing core of vortex ring at left side of reattachment ($Re = 500$, $h/R = 2$)

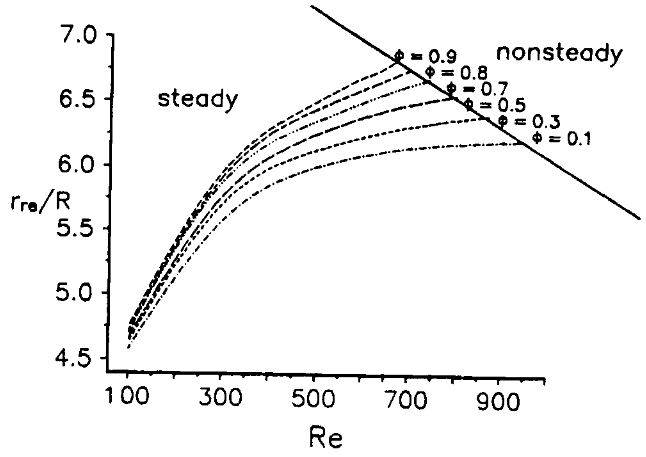

Figure 11. Non-dimensional reattachment radius r_{re}/R as a function of Re for differing upwind fraction Φ ($\Phi = 1$: full central difference)

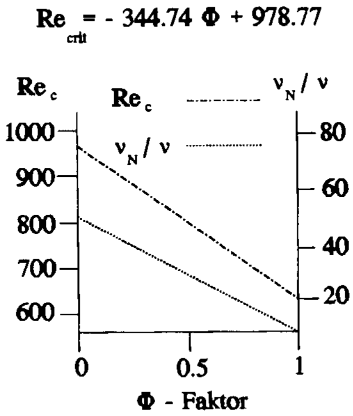

Figure 12. Critical Reynolds number Re_c and fraction of numerical viscosity, ν_N/ν, versus upwind fraction Φ ($\Phi = 1$: full central difference with zero numerical viscosity)

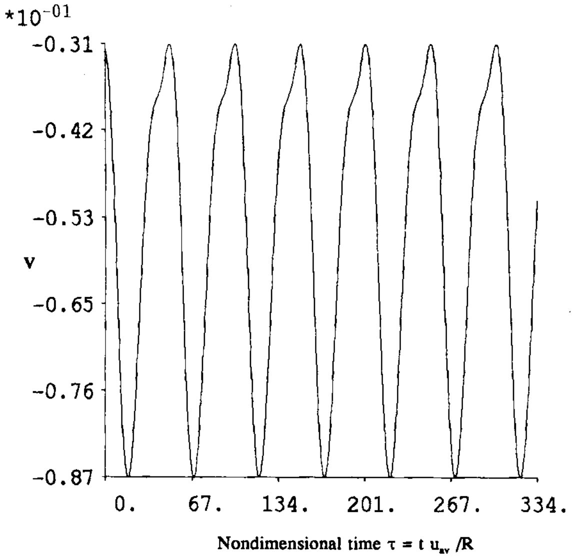

Figure 13. Time series of v-component of velocity at $x/R = 0{\cdot}025$, $r/R = 6{\cdot}5$ ($Re = 720$, $\Phi = 0{\cdot}9$)

almost parallel to the plate and then sharply turns towards the plate at between $r/R = 5$ and 6. Vortices are formed between the impinging plate and the jet and between the top plate and the jet. These vortices guide the jet axis. However, the vortices are not fixed and vortex shedding is observed in successive figures. The vortices even lift the jet slightly from the plate (Figure 15(a5)). Some structural similarity of the flow fields at $\tau = 0$ and 2800 is apparent. However, the time series of the radial velocity v at the chosen point ($x/R = 0{\cdot}025$, $r/R = 6{\cdot}5$) does not indicate periodicity (see Figure 16). Figure 17 shows the Fourier analysis of the time series of Figure 16. A dominant frequency is not present. The flow is possibly chaotic. It should be mentioned here that the present results of the onset of chaos at high Reynolds number should only be treated

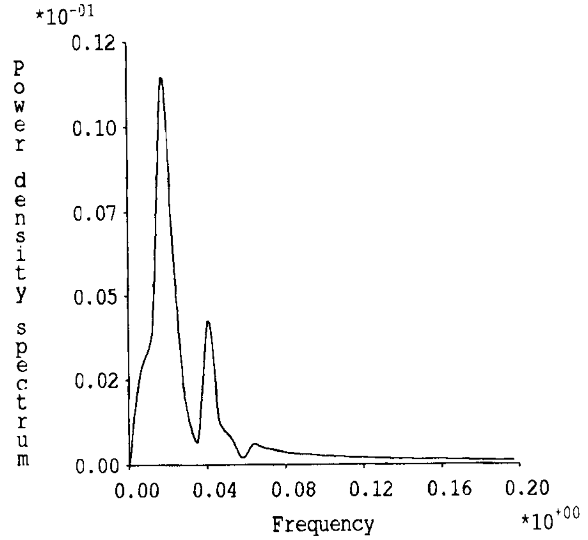

Figure 14. Frequency spectrum obtained from Fourier analysis of time series of Figure 13

as an indication, since the jet flow is assumed axisymmetric. A conclusive study of the onset of chaos will require the simulation of 3D flow.

5. CONCLUSIONS

The computational scheme based on modified SIMPLEC and velocity boundary conditions at the outflow works satisfactorily for radial jet reattachment flow where a flow reversal at the nominal outflow boundary takes place. The flow structure of the reattaching radial jet is highly complex. For a given geometry a critical Reynolds number exists below which a steady flow is obtained. Once *Re* exceeds the critical value, a periodic flow with changing reattachment radius is first obtained. At still higher Reynolds number the periodicity is lost and the flow becomes possibly turbulent. The present study has been carried out for axisymmetric jets. A definitive study of the onset of turbulence indepndence of Reynolds number will of course require a three-dimensional flow investigation.

In the present work the influence of the impingement plate radius L has not been studied. However, some test runs on the influence of L on the flow field were reported in Reference 8. Results for reattaching axial and radial jets computed with $L = 10$ and 15 show that with larger L the vortex between the radial jet and the upper wall becomes more pronounced and influences the reattachment position. For the case where the distance between the upper wall and the jet discharge is smaller than the corresponding distance of the impinging plate the jet still reattaches on the impinging plate for $L = 15$. However, for cases with the upper wall distance larger than the impingement plate distance the flow remains qualitatively the same for $L = 10$ and 15.

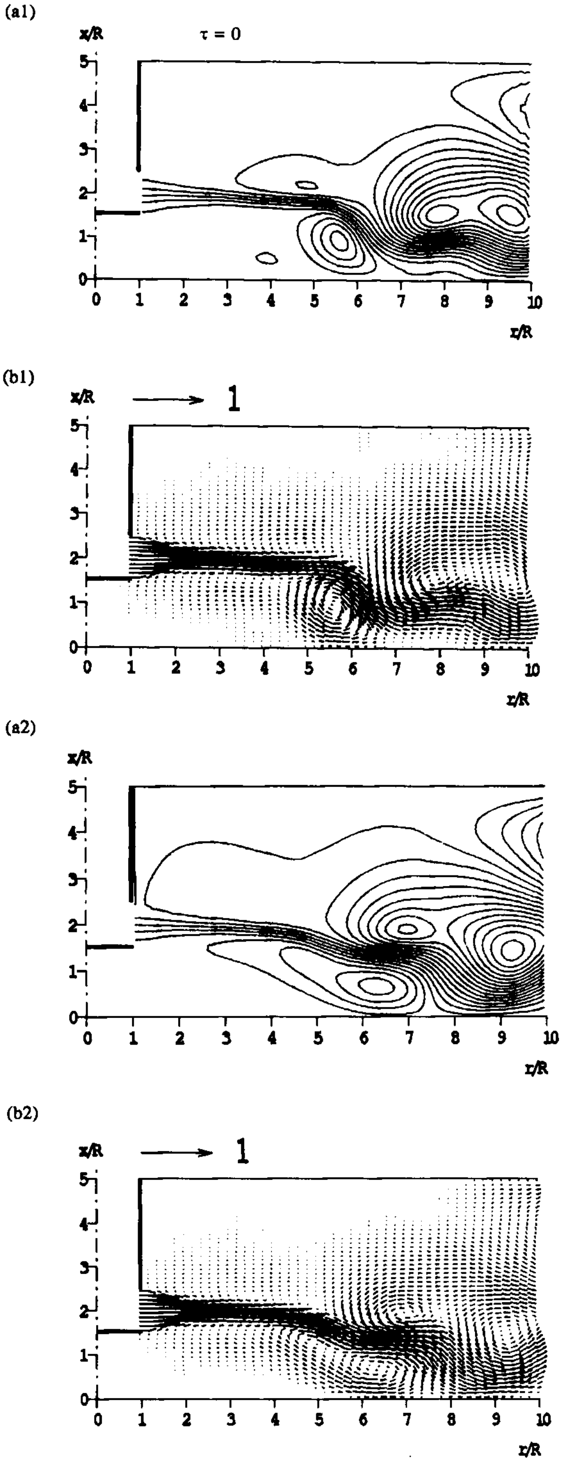

Figure 15. (a) Streaklines and (b) velocity vectors at different times τ for $Re = 800$ ($\Phi = 0{\cdot}9$; typical non-steady non-periodic flow)

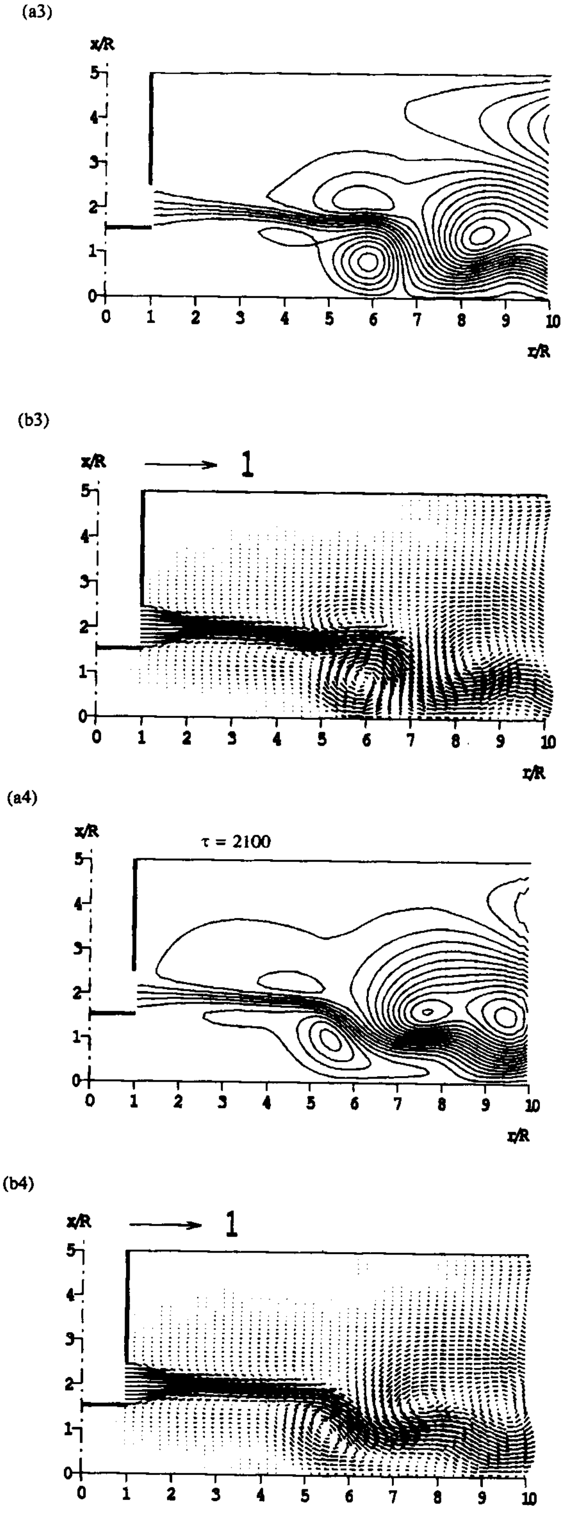

Figure 15 (*continued*)

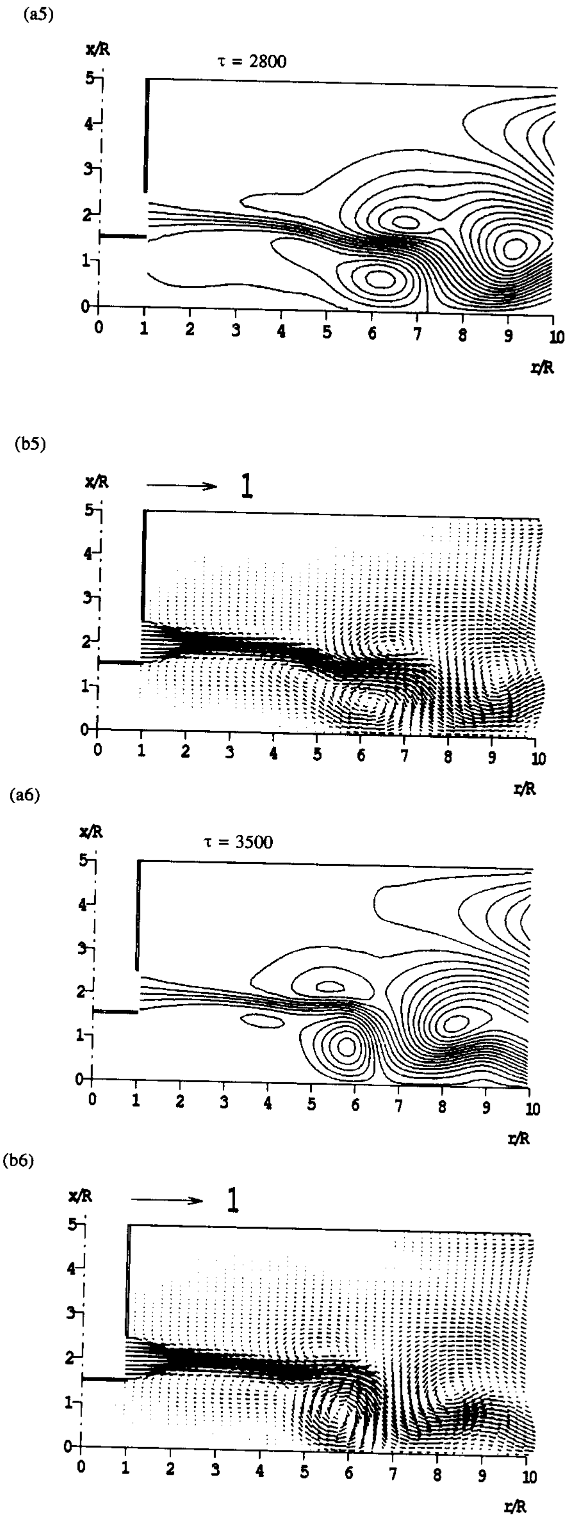

Figure 15 (continued)

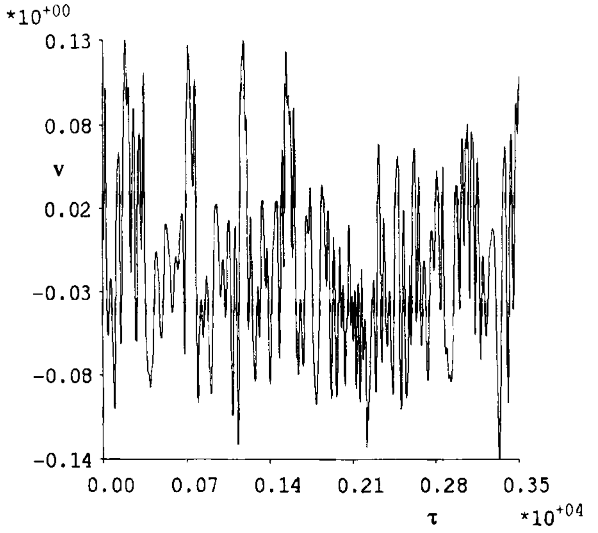

Figure 16. Time series of v-component of velocity at $x/R = 0{\cdot}025$, $r/R = 6{\cdot}5$ ($Re = 800$, $\Phi = 0{\cdot}9$)

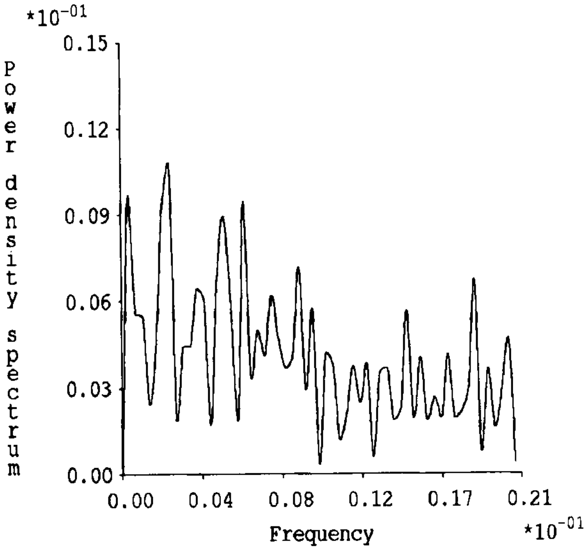

Figure 17. Frequency spectrum obtained from Fourier analysis of time series of Figure 16.

ACKNOWLEDGEMENTS

This work has been supported by the Deutsche Forschungsgemeinschaft.

REFERENCES

1. H. Martin, 'Heat and mass transfer between impinging gas jets and solid surfaces', *Adv. Heat Transfer*, **13**, 1–60 (1977).
2. R. H. Page, L. L. Hadden and C. Ostowari, 'Theory for radial jet reattachment flow', *AIAA J.*, **27**, 1500–1505 (1989).
3. C. Ostowari, B. Paikert and R. H. Page, 'Heat transfer measurement of radial jet reattachment on a flat plate', *Proc. Nat. Fluid Dynamics Congr.*, Cincinnati, OH, July 1988.
4. J. P. van Doormaal and G. D. Raithby, 'Enhancement of the SIMPLE method for predicting incompressible fluid flows', *Numer. Heat Transfer*, **7**, 147–163 (1984).
5. S. V. Patankar, *Numerical Heat Transfer and Fluid Flow*, Hemisphere, Washington, DC, 1980.
6. H. B. Squire, 'Radial jets', in *50 Jahre Grenzschichtforschung*, Vieweg, Braunschweig, 1955, pp. 47–54.
7. R. Rannacher, 'On the numerical solution of incompressible Navier–Stokes equations', *ZAMM*, **73**(9), 203–216 (1993).
8. H. Laschefski, A. Holl, A. Grosse-Gorgemann, N. K. Mitra and R. H. Page, 'Flow structure and heat transfer of a radial and axial jet reattachment on a flat plate', *HTD*, **210**, 123–131 (1992).
9. P. Khosla and S. G. Rubin, 'A diagonally dominant second order accurate implicit scheme', *Comput. Fluids*, **2**, 207–209 (1974).
10. C. R. Maliska and G. D. Raithby, 'A method for computing three dimensional flows using non-orthogonal boundary-fitted coordinates', *Int. j. numer. methods fluids*, **4**, 519–537 (1984).
11. F. H. Harlow and J. E. Welch, 'Numerical calculation of time-dependent viscous incompressible flow', *Phys. Fluids*, **8**, 2182 (1965).
12. C. W. Hirt, B. D. Nichols and N. C. Romero, 'SOLA—a numerical solution algorithm for transient fluid flows', *Los Alamos Scientific Laboratory Rep. LA-5652*, 1975.
13. P. M. Gresho, 'Letter to the Editor', *Numer. Heat Transfer A*, **20**, 123 (1991).
14. S. H. Chuang and C. Y. Wei, 'Computations for a jet impinging oblique on a flat surface', *Int. j. numer. methods fluids*, **12**, 637–653 (1991).